01 Sep 2008

Power System Control with an Embedded Neural Network in Hybrid System Modeling

Seung-Mook Baek

Jung-Wook Park

Ganesh K. Venayagamoorthy
Missouri University of Science and Technology

Recommended Citation

S. Baek et al., "Power System Control with an Embedded Neural Network in Hybrid System Modeling," *IEEE Transactions on Industry Applications*, Institute of Electrical and Electronics Engineers (IEEE), Sep 2008. The definitive version is available at https://doi.org/10.1109/TIA.2008.2002172

Power System Control With an Embedded Neural Network in Hybrid System Modeling

Seung-Mook Baek, *Student Member, IEEE*, Jung-Wook Park, *Member, IEEE*, and
Ganesh Kumar Venayagamoorthy, *Senior Member, IEEE*

Abstract—Output limits of the power system stabilizer (PSS) can improve the system damping performance immediately following a large disturbance. Due to nonsmooth nonlinearities arising from the saturation limits, these values cannot be determined by the conventional tuning methods based on linear analysis. Only *ad hoc* tuning procedures can been used. A feedforward neural network (with a structure of multilayer perceptron neural network) is applied to identify the dynamics of an objective function formed by the states and, thereafter, to compute the gradients required in the nonlinear parameter optimization. Moreover, its derivative information is used to replace that obtained from the trajectory sensitivities based on the hybrid system model with the differential-algebraic-impulsive-switched structure. The optimal output limits of the PSS tuned by the proposed method are evaluated by time-domain simulation in both a single-machine infinite bus system and a multimachine power system.

Index Terms—Feedforward neural network (FFNN), hybrid system, nonlinearities, nonsmoothness, parameter optimization, power system stabilizer (PSS).

I. INTRODUCTION

THE HYBRID systems have recently attracted considerable attention for the researches of many physical systems, which exhibit a mix of continuous dynamics, discrete-time and discrete-event dynamics, switching action, and jump phenomena [1], [2]. For a typical disturbance, power system stabilizer (PSS) used to mitigate system damping of low-frequency oscillations is an important control objective in the hybrid system application because the nonsmooth nonlinear dynamic behaviors due to a saturation limiter fall into a category of the hybrid systems in that an event occurs when a controller signal saturates.

The dynamic behavior of the PSS is affected by linear parameters (the gain and time constants of phase compensator) and constrained parameters (saturation output limits) resulting in nonsmooth nonlinear behavior. The proper selection of linear parameters has been usually made based on conventional tuning techniques by using small-signal stability analysis [3]–[6]. However, by focusing only on small-signal conditions, the dynamic damping performance immediately following a large disturbance is often degraded. The PSS output limits (which cannot be determined by linear approach) can provide a solution to balance these competing effects. In particular, these limit values attempt to prevent the machine terminal voltage from falling below the exciter reference level while speed is also falling. This means that the reduced transient recovery can be improved after a disturbance (faster recovery to its initial steady-state points; therefore, it allows the system to save energy), particularly in multimachine power systems (MMPSs).

In this paper, the hybrid systems applied to the parameter optimization for the PSS output limits are modeled by a set of *differential-algebraic-impulsive-switched* (DAIS) structure as reported in [7], where the derivative information of a model was obtained by the computation of the trajectory sensitivities through the exact modeling of a plant. However, in some practical applications, the exact modeling for a physical nonlinear device (for example, a switching device such as a pulsewidth-modulated inverter) may not be accomplished. Furthermore, the calculation of derivatives of a complex system (such as a large-scale power system) also requires highly computational efforts. Artificial neural network (ANN) can be an alternative to replace the computation of the first-order derivatives from the trajectory sensitivities in the DAIS structure for the hybrid system model, because the ANN is able to adaptively model or identify a nonlinear multiple-input–multiple-output plant without requiring the exact mathematical modeling of plant [8].

This paper makes a new contribution by applying a feedforward neural network (FFNN) to the hybrid system modeling to compute the first-order derivatives required for nonlinear parameter optimization of the PSS in power systems. The performance of the PSS nonlinear controller tuned optimally by the proposed method is assessed by case studies carried out on a single-machine infinite bus system (SMIB) and an MMPS.

II. HYBRID SYSTEM PRESENTATION

As already mentioned, hybrid systems, which include power systems, are characterized by the following:
1) continuous and discrete states;
2) continuous dynamics;
3) discrete events or triggers;
4) mappings that define the evolution of discrete states at events.

S.-M. Baek and J.-W. Park are with the School of Electrical and Electronic Engineering, Yonsei University, Seoul 120-749, Korea (e-mail: sm_baek@yonsei.ac.kr; jungpark@yonsei.ac.kr).

G. K. Venayagamoorthy is with the Department of Electrical and Computer Engineering, Missouri University of Science and Technology, Rolla, MO 65409 USA (e-mail: ganeshv@mst.edu).

In other words, the hybrid system is a mathematical model of physical process consisting of an interacting continuous and discrete event system. A formal presentation of the hybrid system is given in [9], where a general hybrid dynamical system is defined as $H = [Q, \Sigma, A, G]$, where

Q — set of discrete states;

$\Sigma = \{\Sigma_q\}_{q \in Q}$ — collection of dynamical systems $\Sigma_q = [X_q, \Gamma_q, f_q]$, where X_q is an arbitrary topological space forming the continuous state space of Σ_q, Γ_q is a semigroup over which the states evolve, and f_q generates the continuous state dynamics;

$A = \{A_q\}_{q \in Q}$ — $A_q \subset X_q$ for each $q \in Q$ collection of autonomous jump sets, i.e., the conditions which trigger jumps;

$G = \{G_q\}_{q \in Q}$ — where $G_q : A_q \to S = \cup_{q \in Q}(X_q \times \{q\})$ autonomous jump transition map. The hybrid state space of H is given by S.

The aforementioned level of abstraction of the general hybrid system does not suit the implementation of a numerical optimization method carried out in this paper, for which the first-order derivative information can be exploited efficiently. A hybrid model with the DAIS structure, which is more conductive to such analysis, can be presented without loss of generalities as follows [7]:

$$\dot{\underline{x}} = \underline{f}(\underline{x}, y) \tag{1}$$

$$0 = g(\underline{x}, y) \tag{2}$$

$$0 = \begin{cases} g^{(i-)}(\underline{x}, y), & y_{d,i} < 0, \\ g^{(i+)}(\underline{x}, y), & y_{d,i} > 0, \end{cases} \quad i = 1, \dots, d \tag{3}$$

$$\underline{x}^+ = \underline{h}_j(\underline{x}^-, y^-), \qquad y_{e,j} = 0, \quad j \in \{1, \dots, e\} \tag{4}$$

where

$$\underline{x} = \begin{bmatrix} x \\ z \\ \lambda \end{bmatrix}, \quad \underline{f} = \begin{bmatrix} f \\ 0 \\ 0 \end{bmatrix}, \quad \underline{h}_j = \begin{bmatrix} x \\ h_j \\ \lambda \end{bmatrix},$$

$$\underline{x} \in X \subseteq \Re^n, \ y \in Y \subseteq \Re^m, \ z \in Z \subseteq \Re^l, \ \lambda \in L \subseteq \Re^p$$

where

x's — continuous dynamic states, such as generator angles, speed, and fluxes;

z's — discrete dynamic states, such as transformer tap positions and protection relay logic states;

y's — algebraic states, e.g., load bus voltage magnitudes and angles;

λ's — parameters such as generator reactance, controller gains, switching times, and limit values.

The differential equation $\underline{f}$ in (1) is correspondingly structured for $\dot{x} = \underline{f}(x, y)$, while z and λ remain constant away from events. Similarly, the reset equation $\underline{h}_j$ in (4) ensures that x and λ remain constant at reset events, but the dynamic states z's are reset to new values according to $z^+ = h_j(\underline{x}^-, y^-)$. The notation $\underline{x}^+$ denotes the value of $\underline{x}$ just after the reset event, whereas $\underline{x}^-$ and y^- refer to the values of $\underline{x}$ and y, respectively, just prior to the event. The algebraic function g in (2) is composed of $g^{(0)}$
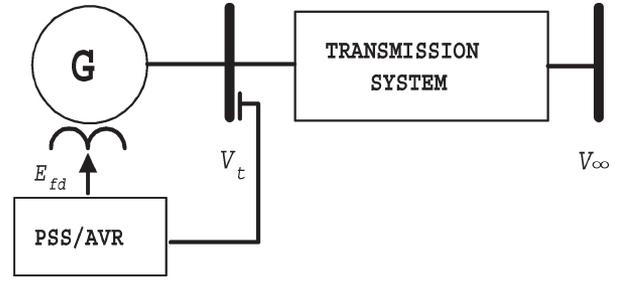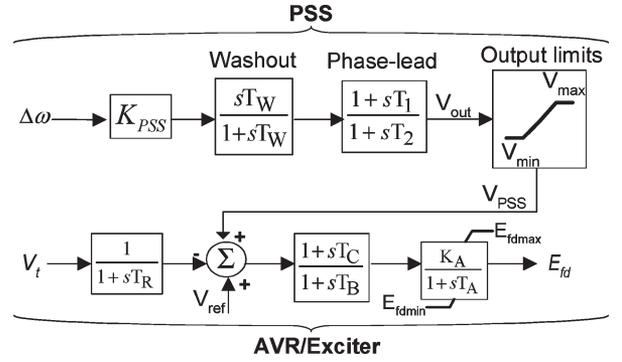

Fig. 1. SMIB.

Fig. 2. AVR/PSS block representation.

together with appropriate choices of $g^{(i-)}$ or $g^{(i+)}$, depending on the signs of the corresponding elements of y_d in (3). An event is triggered by an element of y_d changing sign and/or an element of y_e in (4) passing through zero. In other words, at an event, the composition of g changes, and/or the elements of z are reset. Then, the system flows ϕ are defined accordingly as

$$\phi(\underline{x}_0, t) = \begin{bmatrix} \phi_{\underline{x}}(\underline{x}_0, t) \\ \phi_y(\underline{x}_0, t) \end{bmatrix} = \begin{bmatrix} \underline{x}(t) \\ y(t) \end{bmatrix}. \tag{5}$$

The full detailed explanation and associated mathematical equations of the DAIS model (particularly for the switching and impulse effects) are given in [7] with comprehensive studies of the hybrid system.

III. Nonlinear Controller Optimization

In engineering multivariable nonlinear problems, numerical optimization methods play a significant role in finding solutions of nonlinear functions on complex systems or may select the parameters by which the objective function **J** can be minimized or maximized. The optimal tuning problem for the PSS output limits described in this paper is the case of the latter. Again, in this paper, the gradient information required for the nonlinear parameter optimization is obtained by the FFNN applied to the hybrid system, rather than the computation of the trajectory sensitivities through the exact modeling of a plant.

A. Implementation of Optimal Tuning Applied to PSS

An SMIB is shown in Fig. 1. The PSS and the automatic voltage regulator (AVR) controllers in Fig. 2 are connected to the generator (**G**) of the SMIB system. The generator (**G**)

is accurately represented by a six-order machine model, viz., a two-axis $(d-q)$ model with two damper windings in each axis [10].

In Fig. 2, the output (clipping) limits on the PSS output V_{PSS} and the antiwindup limits on the field voltage E_{fd} introduce events that can be captured by the DAIS model. In other words, the event occurs when a controller signal saturates in response to the large inputs ($\Delta\omega$ and V_{t}) by disturbance. This indicated phenomenon is implemented by the DAIS structure as given in (6) and (7), shown at the bottom of the page, for the PSS clipping limits and the AVR antiwindup limits, respectively.

Many practical optimization problems can be formulated using a Bolza form of the objective function $\mathbf{J}$

$$\min_{\lambda, t_{\mathrm{f}}} \mathbf{J}(\underline{x}, y, \lambda, t_{\mathrm{f}}) \tag{8}$$

subject to $\begin{bmatrix} \underline{x}(t) \\ y(t) \end{bmatrix} = \phi(\underline{x}_0, t)$, where $\underline{x} \in S$ (constraint set)

$$\tag{9}$$

$$\mathbf{J} = \varphi\left(\underline{x}(t_{\mathrm{f}}), y(t_{\mathrm{f}}), \lambda, t_{\mathrm{f}}\right) + \int_{t_0}^{t_{\mathrm{f}}} \psi\left(\underline{x}(t), y(t), \lambda, t\right) dt \tag{10}$$

where λ's are the optimized parameters (output limits in this paper) that are adjusted to minimize the value of objective function $\mathbf{J}$ in (10), and t_{f} is the final time. The objective of tuning PSS controller is to mitigate system damping and force the system to recover to the postdisturbance stable operating point as quickly as possible. The speed deviation ($\Delta\omega$) and the terminal voltage deviation (ΔV_{t}) of the generator in Fig. 2 are considered as good assessments of the damping and recovery [6]. Therefore, the objective function $\mathbf{J}$ in (10) can be reformulated
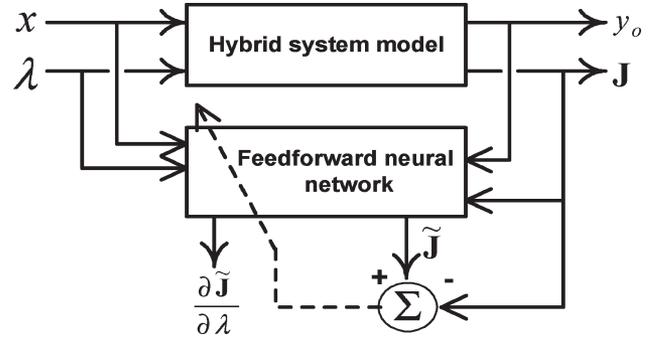

Fig. 3. FFNN applied to the hybrid system.

for the optimal tuning of the PSS with specific time t_{f} as follows:

$$\mathbf{J}(\lambda) = \int_{t_0}^{t_{\mathrm{f}}} \left(\begin{bmatrix} \omega(\lambda, t) - \omega^{\mathrm{s}} \\ V_{\mathrm{t}}(\lambda, t) - V_{\mathrm{t}}^{\mathrm{s}} \end{bmatrix}^{\mathrm{T}} \mathbf{V} \begin{bmatrix} \omega(\lambda, t) - \omega^{\mathrm{s}} \\ V_{\mathrm{t}}(\lambda, t) - V_{\mathrm{t}}^{\mathrm{s}} \end{bmatrix} \right) dt \tag{11}$$

where $\mathbf{V}$ is the weighting matrix, and ω^{s} and $V_{\mathrm{t}}^{\mathrm{s}}$ are the post-fault steady-state values of ω and V_{t}, respectively. Note that the diagonal terms in the matrix $\mathbf{V}$ are determined by considering the balance of conflicting requirements on the speed and voltage deviations.

B. Computation of Gradient by the FFNN

To minimize the value of the function $\mathbf{J}(\lambda)$ in (10), the first-order derivatives of $\mathbf{J}$ with respect to λ ($V_{\max}$ and $V_{\min}$) need to be estimated by the FFNN, as shown in Fig. 3. The proposed

$$y_1 = V_{\max} - V_{\mathrm{out}}$$

$$y_2 = V_{\mathrm{out}} - V_{\min}$$

$$0 = \begin{cases} g_1^{(i-)}(\underline{x}, y) = V_{\mathrm{PSS}} - V_{\max}, & y_1 < 0 \\ g_1^{(i-)}(\underline{x}, y) = V_{\mathrm{PSS}} - V_{\min}, & y_2 < 0 \\ g_1^{(i+)}(\underline{x}, y) = g_2^{(i+)}(\underline{x}, y) = V_{\mathrm{PSS}} - V_{\mathrm{out}}, & y_1 > 0, \ y_2 > 0 \end{cases}$$

$$\tag{6}$$

$$y_3 = E_{\mathrm{fdmax}} - E_{\mathrm{fd}};$$

$$\quad y_4 (\text{upper limits switch}) : (+\text{when } y_3 < 0)$$

$$y_5 = E_{\mathrm{fd}} - E_{\mathrm{fdmin}};$$

$$\quad y_6 (\text{lower limits switch}) : (+\text{when } y_5 < 0)$$

$$0 = \begin{cases} g_3^{(i-)}(\underline{x}, y) = y_4 - 1, & y_3 < 0 \\ g_4^{(i-)}(\underline{x}, y) = E_{\mathrm{fd}} - E_{\mathrm{fdmax}}, & y_3 < 0 \\ g_5^{(i-)}(\underline{x}, y) = y_6 - 1, & y_5 < 0 \\ g_6^{(i-)}(\underline{x}, y) = E_{\mathrm{fd}} - E_{\mathrm{fdmin}}, & y_5 < 0 \\ g_3^{(i+)}(\underline{x}, y) = g_5^{(i+)}(\underline{x}, y) = y_4 = y_6, & y_3 > 0, \ y_5 > 0 \\ g_4^{(i+)}(\underline{x}, y) = g_6^{(i+)}(\underline{x}, y) = K_{\mathrm{A}} \cdot x_{\mathrm{trg}} - E_{\mathrm{fd}}, & y_3 > 0, \ y_5 > 0 \end{cases}$$

$$\tag{7}$$

Fig. 4.   Structure of the FFNN.

Fig. 5.   Identification of the function **J** by the FFNN.
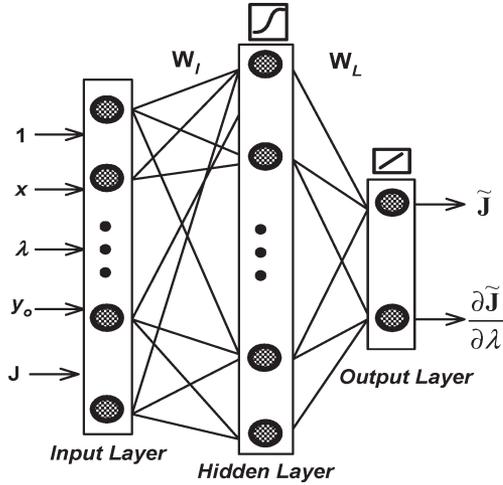
FFNN (with the multilayer perceptron structure) consists of three layers (input, hidden, and output layers) of neurons in Fig. 4 interconnected by the weight matrices $\mathbf{W}_l$ and $\mathbf{W}_L$. It is firstly designed to identify the dynamics of the plant. The activation function for neurons in the hidden layer in Fig. 4 is given by the following sigmoidal function:

$$s(x) = \frac{1}{1 + \exp(-x)}. \tag{12}$$

The output layer neurons are formed by the inner products between the nonlinear regression vector from the hidden layer and the output weight matrix. Generally, the FFNN starts with random initial values for its weights and then computes a one-pass backpropagation algorithm [11] at each time step k, which consists of a forward pass propagating the input vector through the network layer by layer and a backward pass to update the weights with the error signal between **J** and $\tilde{\mathbf{J}}$, as shown in Fig. 3.

The functional expression ζ of the FFNN used for this paper is given as

$$\left(\tilde{\mathbf{J}}(k), \frac{\partial \tilde{\mathbf{J}}}{\partial \lambda}(k)\right) = \zeta\left(x(k-1), y_{\mathrm{o}}(k-1), \lambda(k-1), \mathbf{J}(k-1)\right) \tag{13}$$

where
k denotes the time index;
x $= [\Delta\omega, \Delta V_{\mathrm{t}}]$;
y_{o} $= V_{\mathrm{PSS}}$ (in Fig. 2);
λ $= [V_{\max} V_{\min}]$ (in Fig. 2);
J   output of the objective function defined in (11).

After training the weights of the FFNN offline for 100 s (in simulation time), the identification performance of the function **J** by the FFNN is evaluated. The result is shown in Fig. 5, where the values of **J** are the corresponding responses when a large disturbance (a 100-ms three-phase short circuit) is applied to the generator terminal bus in Fig. 2 at $t = 0.05$ s. Moreover, the final time t_{f} in (11) is 5 s. It is obvious from this result that the

Fig. 6.   Values of $\partial \tilde{\mathbf{J}}/\partial V_{\max}$ by the FFNN at each iteration.

FFNN is able to identify the objective function **J** with sufficient accuracy.

Thereafter, the gradient $\nabla\tilde{\mathbf{J}}(\lambda) = \partial\tilde{\mathbf{J}}/\partial\lambda$ is calculated by the back-stepping computation based on chain rule through the FFNN [11] and is given as

$$\nabla\tilde{\mathbf{J}}(\lambda) = \frac{\partial\tilde{\mathbf{J}}}{\partial\lambda} = \frac{\partial\tilde{\mathbf{J}}}{\partial t}\frac{\partial t}{\partial p_L}\frac{\partial p_L}{\partial q_L}\frac{\partial q_L}{\partial p_l}\frac{\partial p_l}{\partial q_l}\frac{\partial q_l}{\partial\lambda}$$

$$= \{s(q_l)(1 - s(q_l))\mathbf{W}_l(\lambda)\}\sum_{j=1}^{m_l}\tilde{\mathbf{J}}\cdot\mathbf{W}_L \tag{14}$$

where
t target value;
m_l number of neurons in the hidden layer;
p output of the activation function for a neuron;
q regression vector given as the activity of a neuron;
$\mathbf{W}$ weight matrix;
L and l output and hidden layers, respectively;
s sigmoidal function in (12).

The variations of $\nabla\tilde{\mathbf{J}}(\lambda) = \partial\tilde{\mathbf{J}}/\partial\lambda$ for the nonlinear parameters $V_{\max}$ and $V_{\min}$ at each iteration are shown in Figs. 6 and 7, respectively. Then, these nonlinear parameters λ are updated
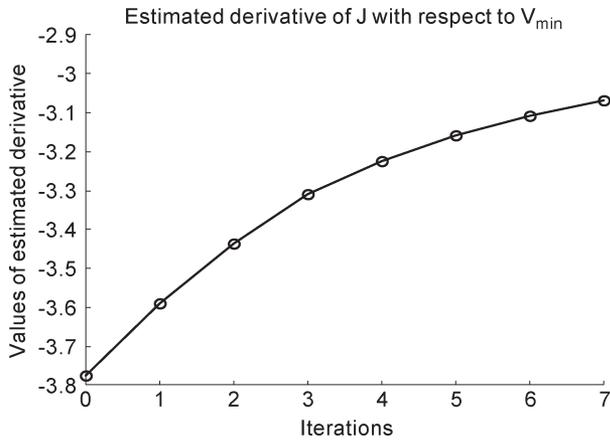
Fig. 7. Values of $\partial \tilde{\mathbf{J}}/\partial V_{\min}$ by the FFNN at each iteration.

by using (15) with $\nabla \tilde{\mathbf{J}}(\lambda)$ during iteration. It is clearly shown from Figs. 6 and 7 that the absolute values of gradients are decreased after each iteration and converged to their optimal local minimum in the suboptimal space formed when applying the large disturbance (three-phase short circuit) to the plant

$$\lambda_{k+1} = \lambda_k + \alpha \cdot \nabla \tilde{\mathbf{J}}(\lambda) \qquad (15)$$

where α is the step length.

At the end of each run, convergence performance is evaluated by the user-defined criterion, which are the maximum relative changes in parameters (S_C) as given in (16) as well as the value of $\mathbf{J}$. Note that the parameter optimization problem by the FFNN aims to minimize the value of objective function $\mathbf{J}(\lambda)$ with a small number of iterations

$$S_C = \left\| \frac{\lambda_{k+1} - \lambda_k}{\lambda_{k+1}} \right\|_\infty . \qquad (16)$$

C. Optimization Algorithm and Simulation Program Interface

Fig. 8 shows the flow diagram to interface the proposed optimization algorithm with the simulation program used in this paper, which is the MATLAB software. The entire optimization process is carried out in several successive simulation runs, which is called as iterations, i.e., one complete simulation run is dedicated to the candidate solution of λ for the simulation run [12], [13].

IV. CASE STUDIES

A. Test in SMIB

During the optimization process (iteration) applied to the SMIB system in Fig. 1, the values of the objective function $\mathbf{J}$ variations are shown in Fig. 9. The FFNN is successfully applied to the hybrid system model for the PSS output limits, thus minimizing the values of $\mathbf{J}$ in this nonlinear parameter optimization problem. The corresponding maximum relative changes (S_C) in (16) at each iteration are also shown in Fig. 10. It may be valuable to compare the convergence speed by any
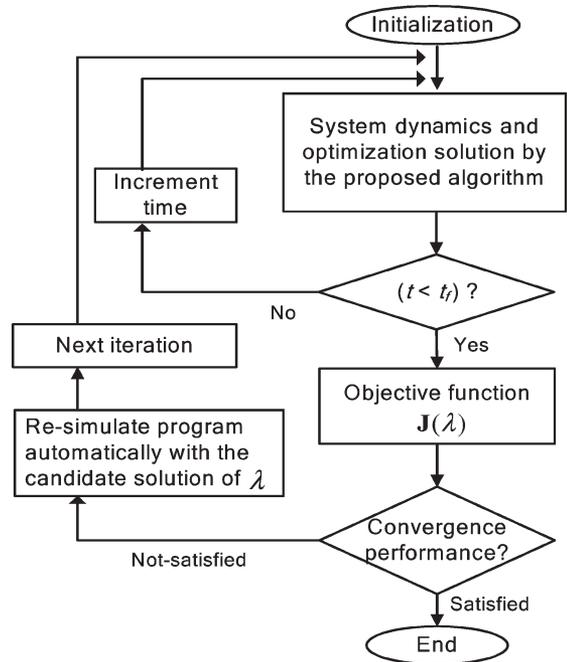

Fig. 8. Flow diagram of the proposed optimization algorithm and simulation program interface.

Fig. 9. Values of the objective function $\mathbf{J}$ variations.
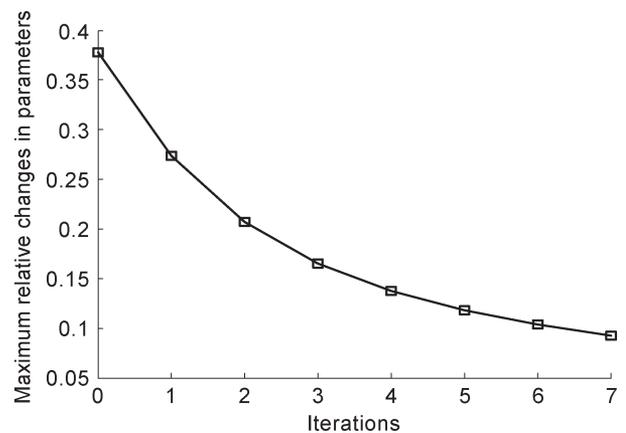
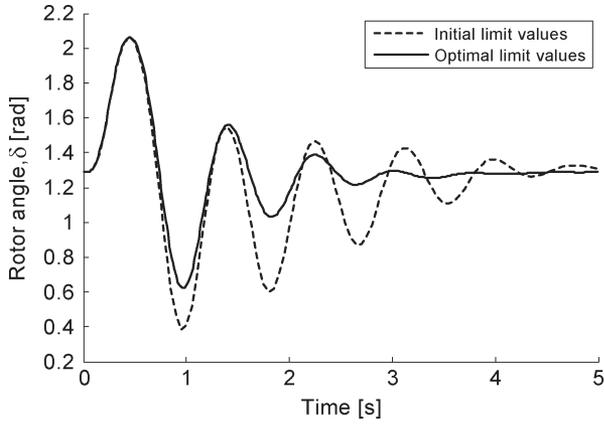

Fig. 10. Maximum relative changes in the optimized parameters.
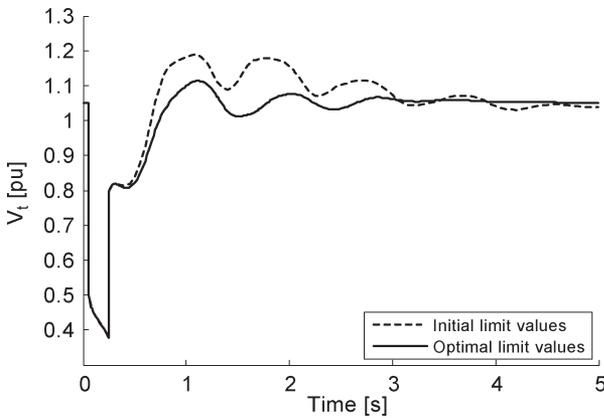
Fig. 11. Generator rotor angle response (in radians).

Fig. 12. Generator terminal voltage response (in per unit).

Fig. 13. PSS output response.

Fig. 14. Four-machine two-area test system.

other improved numerical optimization such as the conjugate-gradient or quasi-Newton methods.

The damping performance of the output limits (which are [0.1105 −0.3365] for [$V_{max} V_{min}$]) of the PSS optimized after seven iterations is compared with that of the initial output limits [0.1 −0.1] by applying the 100-ms three-phase fault at the generator terminal bus in Fig. 1 at 0.05 s. The simulation results are shown in Figs. 11 and 12. It is clearly shown that the optimal saturation limits determined by the proposed method effectively improve the system dynamic damping and transient terminal voltage response. The value of V_{max} has been slightly changed from 0.1 to 0.1105, but the value of V_{min} has moved significantly from −0.1 to −0.3365. The effect of optimal tuning for these saturation limits is rather dramatic and quite evident for a large disturbance (such as a three-phase short circuit) applied to a power system. The corresponding PSS output response (V_{PSS}) in Fig. 13 exhibits the nonsmooth nonlinear dynamic behaviors. Note that a lowering of V_{min} is quite counterintuitive; manual tuning would likely not even search in that direction for an improved response.

B. Test in MMPS

The IEEE benchmark four-machine two-area test system is shown in Fig. 14. The data of this system are given in [6]. Each machine has been presented by a fourth-order nonlinear
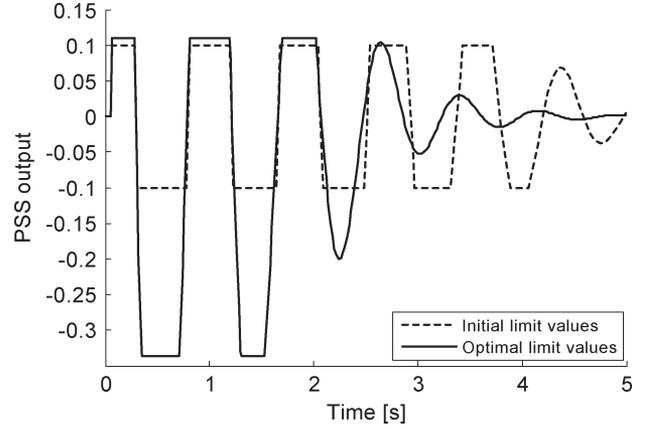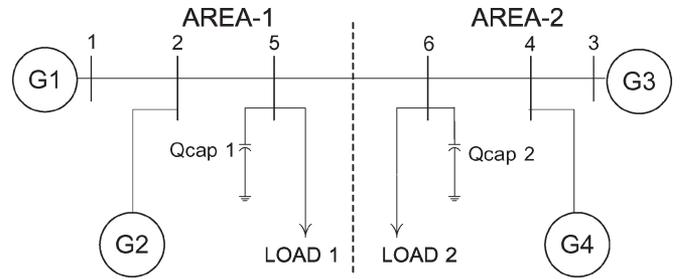
model [10]. All generators (G1–G4) are equipped with the AVR/PSS system shown in Fig. 2.

The effect of the optimal limit values of the multi-PSSs on the MMPS in Fig. 14 with respect to the damping performance is investigated. The objective function **J** in (11) is redefined for the application to the MMPS as

$$\mathbf{J}(\lambda) = \sum_{i=1}^{4} \int_{t_0}^{t_f} \left(\begin{bmatrix} \omega_i(\lambda,t) - \omega_i^s \\ V_{t,i}(\lambda,t) - V_{t,i}^s \end{bmatrix}^{\mathrm{T}} \mathbf{V} \begin{bmatrix} \omega_i(\lambda,t) - \omega_i^s \\ V_{t,i}(\lambda,t) - V_{t,i}^s \end{bmatrix} \right) dt$$
(17)

where the subscript i is the generator number in Fig. 14.

While minimizing the single value of function **J** in (17), the proposed method is applied to determine the optimal output limits of the local PSSs, which are affected by the interactions with each other on the multimachine power network. This application gives a good example for the *global dynamic optimization* of large-scale complex systems.

A total of 21 inputs and 36 neurons are used in the input and hidden layers of the FFNN, respectively. As the procedure described in Section III, after training the weights of the FFNN offline, the parameters λ (output limits of all PSSs) are updated by (15) with the gradients $\nabla \tilde{\mathbf{J}}(\lambda) = \partial \tilde{\mathbf{J}}/\partial \lambda$ computed through the FFNN by (14) during the optimization process.

It is clearly shown from Fig. 15 that the values of the objective function **J**, which correspond to the updated parameters, are minimized at each iteration. After ten iterations in Fig. 15, the values of the optimized output limits are given in Table I with those of the initial output limits.
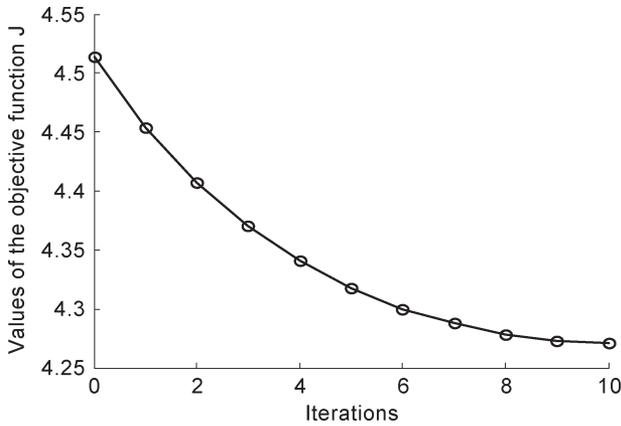
Fig. 15.   Values of the objective function **J** variations: test on the MMPS.

TABLE I
INITIAL VERSUS OPTIMAL LIMIT VALUES OF PSSs

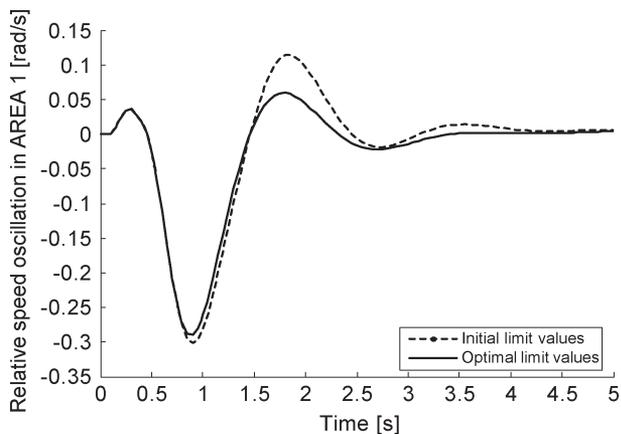| Output limits	Initial [V_{max} V_{min}]	Optimal [V_{max} V_{min}]
PSS-G1	[0.05 −0.05]	[0.0992 −0.1268]
PSS-G2	[0.05 −0.05]	[0.1021 −0.0828]
PSS-G3	[0.1 −0.1]	[0.1533 −0.2558]
PSS-G4	[0.1 −0.1]	[0.1484 −0.1938]

Fig. 16.   Relative speed oscillations ($\Delta\omega_1 - \Delta\omega_2$) in AREA-1 (in radians per second).

The damping performance by the PSSs with the optimized output limits is evaluated by applying the 150-ms three-phase fault at bus 5 in Fig. 14 at 0.1 s. The relative speed oscillations ($\Delta\omega_1 - \Delta\omega_2$ and $\Delta\omega_3 - \Delta\omega_4$) for the deviation signals in AREA-1 and AREA-2 are given in Figs. 16 and 17, respectively. In addition, the relative speed oscillation ($\Delta\omega_1 - \Delta\omega_3$) in interarea mode between AREA-1 and AREA-2 is shown in Fig. 18. The simulation results show that the dynamic performance to damp out the low-frequency oscillations is effectively improved by the optimized output limits, which are nonsmooth nonlinear parameters. In particular, the damping in AREA-2 is remarkably improved compared with that in AREA-1. Correspondingly, the parameter variations in AREA-2 are higher than those in AREA-1 (see Table I).
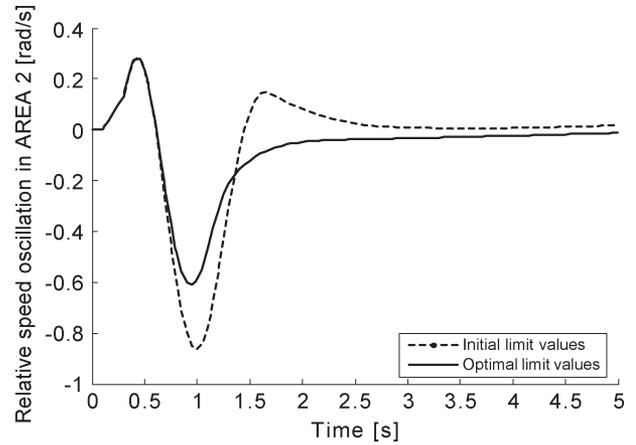

Fig. 17.   Relative speed oscillations ($\Delta\omega_3 - \Delta\omega_4$) in AREA-2 (in radians per second).
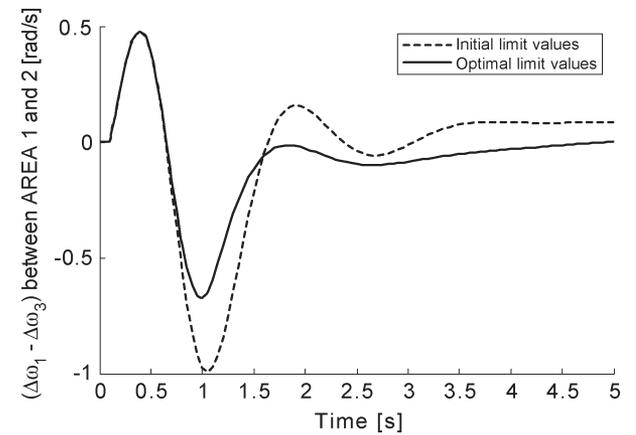

Fig. 18.   Relative speed oscillations ($\Delta\omega_1 - \Delta\omega_3$) in interarea mode between AREA-1 and AREA-2 (in radians per second).

V. CONCLUSION

In this paper, the output limits of the PSS in a power system were considered as the parameters to be optimized by using the hybrid system model with the DAIS structure. To implement the nonlinear parameter optimization, the FFNN was applied to the hybrid system model to compute the gradients of the objective function **J** with respect to the PSS output limits. In other words, the FFNN was used as an alternative to replace the computation of the first-order derivatives from the trajectory sensitivities. Therefore, the main contribution of this paper is to apply the hybrid system that combines analytical modeling with the soft-computing method such as an ANN to the power system control.

Availability of the FFNN in the hybrid system modeling makes it possible to avoid the exact modeling of the overall plant and, thereby, to reduce the computational efforts required in a large-scale complex hybrid system. It is still an open question as to which gradient-based method is the most appropriate. The steepest descent method by the gradients computed through the FFNN may require many iterations with low convergence speed. This situation can be avoided by the conjugate-gradient and quasi-Newton type methods, which provide an estimate of the second derivatives.

ACKNOWLEDGMENT

REFERENCES

[1] A. van der Schaft and H. Schumacher, *An Introduction to Hybrid Dynamical Systems*. London, U.K.: Springer-Verlag, 2000.

[2] D. Liberzon, *Switching in Systems and Control*. Boston, MA: Birkhauser, 2003.

[3] P. Kundur, M. Klein, G. J. Rogers, and M. S. Zywno, "Application of power system stabilizers for enhancement of overall system stability," *IEEE Trans. Power Syst.*, vol. 4, no. 2, pp. 614–626, May 1989.

[4] M. Klein, G. J. Rogers, S. Moorty, and P. Kundur, "Analytical investigation of factors influencing power system stabilizers performance," *IEEE Trans. Energy Convers.*, vol. 7, no. 3, pp. 382–388, Sep. 1992.

[5] N. Martins and L. T. G. Lima, "Determination of suitable locations for power system stabilizers and static VAR compensators for damping electromechanical oscillations in large scale power systems," in *Proc. Power Ind. Comput. Appl.*, May 1989, pp. 74–82.

[6] P. Kundur, *Power System Stability and Control*. New York: McGraw-Hill, 1993.

[7] I. A. Hiskens and M. A. Pai, "Trajectory sensitivity analysis of hybrid systems," *IEEE Trans. Circuits Syst. I, Fundam. Theory Appl.*, vol. 47, no. 2, pp. 204–220, Feb. 2000.

[8] K. Narendra and K. Parthasarathy, "Identification and control of dynamical systems using neural networks," *IEEE Trans. Neural Netw.*, vol. 1, no. 1, pp. 4–27, Mar. 1990.

[9] M. S. Branicky, V. S. Borkar, and S. K. Mitter, "A unified framework for hybrid control: Model and optimal control theory," *IEEE Trans. Autom. Control*, vol. 43, no. 1, pp. 31–45, Jan. 1998.

[10] P. W. Sauer and M. A. Pai, *Power System Dynamics and Stability*. Englewood Cliffs, NJ: Prentice-Hall, 1998.

[11] J.-W. Park, G. K. Venayagamoorthy, and R. G. Harley, "MLP/RBF neural-networks-based online global model identification of synchronous generator," *IEEE Trans. Ind. Electron.*, vol. 52, no. 6, pp. 1685–1695, Dec. 2005.

[12] A. M. Gloe, S. Filizadeh, R. W. Menzies, and P. L. Wilson, "Optimization-enabled electromagnetic transient simulation," *IEEE Trans. Power Del.*, vol. 20, no. 1, pp. 512–518, Jan. 2005.

[13] B. H. Kim, "A study on the convergency property of the auxiliary problem principle," *J. Elect. Eng. Technol.*, vol. 1, no. 4, pp. 455–460, 2006.

Jung-Wook Park (S'00–M'03) was born in Seoul, Korea. He received the B.S. degree (*summa cum laude*) from the Department of Electrical Engineering, Yonsei University, Seoul, in 1999, and the M.S. degree in electrical and computer engineering and the Ph.D. degree from the School of Electrical and Computer Engineering, Georgia Institute of Technology, Atlanta, in 2000 and 2003, respectively.

He was a Postdoctoral Research Associate with the Department of Electrical and Computer Engineering, University of Wisconsin, Madison, from 2003 to 2004, and a Senior Research Engineer with LG Electronics Inc., Korea, from 2004 to 2005. He is currently an Assistant Professor with the School of Electrical and Electronic Engineering, Yonsei University. His current research interests include power system dynamics, flexible ac transmission system devices, inverter systems, hybrid systems, optimization control algorithms, and application of artificial neural networks.

Prof. Park was a Technical Cochair of the Power Systems and Power Electronic Circuits Committee, IEEE International Symposium on Circuits and Systems, held in Kobe, Japan, in May 2005. He is currently a member of the Task Force on Intelligent Control Systems Subcommittee of the IEEE Power Engineering Society. He was the recipient of the IEEE Industry Applications Society Second Prize Paper Award in 2003. He is named in the 2006–2007 edition of *Marquis Who's Who in Science and Engineering*, the 2007–2008 edition of *Marquis Who's Who in the World*, USA, the 2007 inaugural edition of *IBC Outstanding Scientists of the 21st Worldwide*, and the *TOP 100 Scientists 2007 in IBC*, U.K.

Ganesh Kumar Venayagamoorthy (S'91–M'97–SM'02) received the B.Eng. degree (Hons.) in electrical and electronics engineering from Abubakar Tafawa Balewa University, Bauchi, Nigeria, in 1994, and the M.Sc.Eng. and Ph.D. degrees in electrical engineering from the University of Natal, Durban, South Africa, in 1999 and 2002, respectively.

He was a Senior Lecturer with Durban Institute of Technology, Durban, prior to joining the Missouri University of Science and Technology (MST), Rolla, in 2002. He was a Visiting Researcher with ABB Corporate Research, Sweden, in 2007. He is currently an Associate Professor with the Department of Electrical and Computer Engineering and the Director of the Real-Time Power and Intelligent Systems Laboratory, MST. His research interests include development and applications of computational intelligence for real-world applications, including power system stability and control, flexible ac transmission system devices, power electronics, alternative sources of energy, sensor networks, collective robotic search, signal processing, and evolvable hardware.

Dr. Venayagamoorthy is currently a Senior Member of the South African Institute of Electrical Engineers (SAIEE). He is also a member of the International Neural Network Society (INNS), The Institution of Engineering and Technology, U.K., and the American Society for Engineering Education. He was an Associate Editor of the IEEE TRANSACTIONS ON NEURAL NETWORKS (2004–2007) and the IEEE TRANSACTIONS ON INSTRUMENTATION AND MEASUREMENT (2007). He is currently the Chapter Chair of the IEEE St. Louis Computational Intelligence Society (CIS) and the IEEE Industry Applications Society (IAS), the Chair of the Working Group on Intelligent Control Systems, the Secretary of the Intelligent Systems subcommittee, the Vice-Chair of the Student Meeting Activities subcommittee of the IEEE Power Engineering Society, and the Chair of the IEEE CIS Task Force on Power System Applications. He has organized and chaired several panels, invited and regular sessions, and tutorials at international conferences and workshops. He was the recipient of the 2007 U.S. Office of Naval Research Young Investigator Program Award, the 2004 NSF CAREER Award, the 2006 IEEE Power Engineering Society Walter Fee Outstanding Young Engineer Award, the 2006 IEEE St. Louis Section Outstanding Section Member Award, the 2005 IEEE IAS Outstanding Young Member Award, the 2005 SAIEE Young Achievers Award, the 2004 IEEE St. Louis Section Outstanding Young Engineer Award, the 2003 INNS Young Investigator Award, the 2001 IEEE CIS Walter Karplus Summer Research Award, five prize papers from the IEEE IAS and IEEE CIS, a 2007 MST Teaching Commendation Award, a 2006 MST School of Engineering Teaching Excellence Award, and a 2007/2005 MST Faculty Excellence Award. He is listed in the 2007 and 2008 editions of *Who's Who in America*, the 2008 edition of *Who's Who in the World*, and the 2008 edition of *Who's Who in Science and Engineering*.

Seung-Mook Baek (S'06) was born in Seoul, Korea. He received the B.S. and M.S. degrees from the School of Electrical and Electronic Engineering, Yonsei University, Seoul, in 2006 and 2007, respectively, where he is currently working toward the Ph.D. degree.

His research interests include power system dynamics, hybrid systems, optimization control algorithms, flexible ac transmission system devices, and control of distributed generations.